ChemComm

Accepted Manuscript

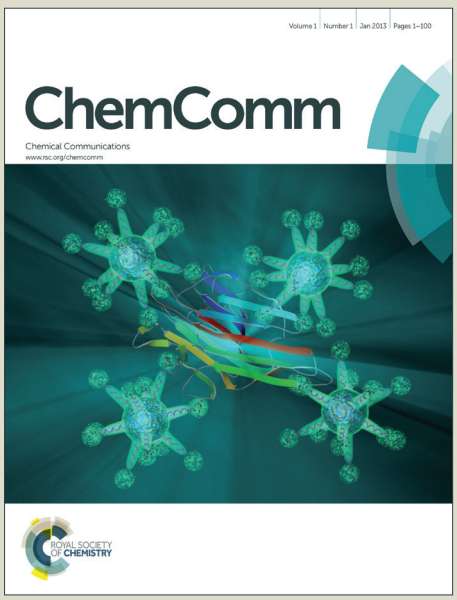

ROYAL SOCIETY OF CHEMISTRY

www.rsc.org/chemcomm

Cite this: DOI: 10.1039/c0xx00000x

www.rsc.org/xxxxxx

COMMUNICATION

Incorporation of heterostructured Sn/SnO nanoparticles in crumpled nitrogen-doped graphene nanosheets as anode for lithium-ion batteries

Fei-Hu Du, Yu-Si Liu, Jie Long, Qian-Cheng Zhu, Kai-Xue Wang,* Xiao Wei* and Jie-Sheng Chen

Received (in XXX, XXX) XthXXXXXXXXX 20XX, Accepted Xth XXXXXXXXX 20XX

DOI: 10.1039/b000000x

Sn/SnO nanoparticles are incorporated in crumpled nitrogen-doped graphene nanosheets by a simple melting diffusion method. The resulting composite exhibits large specific capacity, excellent cycling stability and high rate capability as anode for lithium-ion batteries.

Lithium-ion batteries (LIBs) which have been intensively utilized in portable electronics show significant promise for application in electric vehicles, hybrid electric vehicles and smart grids.[1] Metallic Sn and its oxides with features of high theoretical capacities, low discharge potential, natural abundance, and environmental friendliness have attracted considerable attention and been regarded as potential substitutes for commercial graphite anode.[2] However, the practical implementation of metallic Sn and its oxides suffers from pulverization problem caused by the large volume change (>300%) during lithiation/delithiation processes, which would result in the loss of electrical conductivity and consequently a rapid capacity fading during cycling.[3] The encapsulation in various carbon matrixes,[4] including hollow nanofibers, hollow nanospheres, nanotubes and porous structures, have been proposed to enhance the electrochemical performance of Sn-based nanoparticles. The carbon matrixes can prevent the serious aggregation of the nanoparticles, buffer the volume variation, and maintain the electronic contact among the nanoparticles upon cycling. However, toxic organotin precursors, special devices, harsh reaction conditions or multi-step procedures are usually involved in the preparation of Sn-based nanocomposites, hindering their mass production.[5]

Nazar et al. reported a simple melting diffusion strategy to prepare the CMK-3/S composite cathode for lithium-sulphur batteries.[6] The composite exhibited highly desirable electrochemical characteristics. Recently, metal oxides with relatively low melting points, such as V_2O_5 and MoO_3, were penetrated into mesoporous carbon through capillary forces, generating nanocomposites with controlled morphologies and attractive electrochemical performance.[7] Given the fact that metal Sn has a low melting point of only 231 ºC, it is quite feasible to incorporate Sn into a carbon matrix *via* the melting diffusion strategy at low temperature to obtain Sn-based composite. In this communication, highly crumpled nitrogen-doped graphene nanosheets (NGNSs) with large pore volume and excellent conductivity were employed as a carbon matrix. A composite composed of Sn, SnO and NGNSs (Sn/SnO/NGNSs) was fabricated through simply heating a mixture of commercial Sn nanoparticles and NGNSs, and the resulting composite material exhibited excellent electrochemical performance.

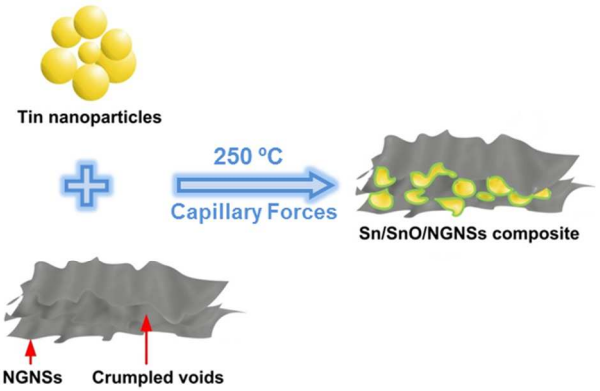

Fig. 1 Schematic illustration of the preparation process of Sn/SnO/NGNSs composite.

The typical procedure for the preparation of the Sn/SnO/NGNSs composite is shown in Fig. 1 (experimental details in ESI†). First, the crumpled NGNSs were prepared following a procedure reported in the literature.[8] Then, Sn nanoparticles (0.3 g) and NGNSs (0.2 g) were mixed together and heated in Ar at a temperature of 250 ºC, about 20 ºC above the melting point of Sn (231 ºC). The molten Sn was gradually imbibed into the pores of NGNSs by capillary forces and partly reacted with the surface functional groups of NGNSs, leading to the formation of the Sn/SnO/NGNSs composite.

The NGNSs have an ultrahigh pore volume and large specific surface area of 2.8 $cm^3\ g^{-1}$ and 721 $m^2\ g^{-1}$, respectively, as evaluated by N_2 adsorption/desorption analysis, much higher than those of the most reported nanostructured carbons, such as mesoporous carbon and carbon nanotubes (Fig. S1, ESI†). After Sn impregnation, the pore volume of the sample decreases to approximately 0.7 $cm^3\ g^{-1}$, indicating that most of the void space within the NGNSs is filled by Sn species (Fig. 2a). The remaining porosity in the resulting Sn/SnO/NGNSs composite is essential for ensuring the fast mass transportation and for accommodating the huge volume change upon alloying and dealloying with lithium. The large BET surface area of the composite remains to be as high as 239 $m^2\ g^{-1}$, ensuring fast electrode kinetics. X-ray diffraction (XRD) pattern of the Sn/SnO/NGNSs composite is shown in Fig. 2b. The diffraction peaks can be well indexed to

tetragonal Sn with a space group of $I4_1/amd$ (JCPDS card No.

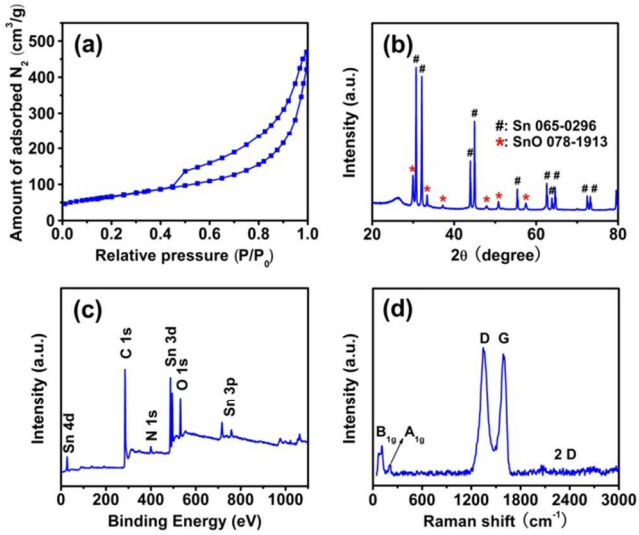

Fig. 2 (a) Nitrogen adsorption-desorption isotherm and pore size distribution curve (inset), (b) XRD pattern, (c) XPS survey scan, and (d) Raman spectrum of the Sn/SnO/NGNSs composite.

065-0296) and tetragonal SnO with a space group of $P4/nmm$ (JCPDS card No. 078-1913), indicating the presence of both metallic Sn and SnO in the composite. The generation of Sn and SnO heterostructure might be due to the reaction of the molten Sn with residual oxygen functional groups of NGNSs. The existence of such functional groups is demonstrated by the X-ray photoelectron spectroscopy (XPS) analysis (Fig. S2a, ESI†). Employing porous carbon without surface oxygen functional groups as a scaffold, no SnO can be generated. It is believed that the formation of SnO leads to tight contact between the nanoparticles and NGNSs.[1a,9] The small broad peak located at approximately 26º in the XRD pattern is ascribed to the (002) reflection of multi-layered NGNSs. The contents of Sn, SnO and NGNSs in the composite determined by semi-quantitative XRD and thermo-gravimetric (TG) analyses are approximately 53, 9, and 38 wt%, respectively (Fig. S3, ESI†). The XPS survey spectrum indicates that the Sn/SnO/NGNSs composite is composed of Sn, C, O, and N elements (Fig. 2c). The Sn 3d spectrum (Fig. S2b, ESI†) shows two peaks at 487.2 eV (Sn $3d_{5/2}$) and 495.6 eV (Sn $3d_{3/2}$), characteristic for tin oxides. Based on the XPS and XRD analyses, it is proposed that SnO is generated on the surface of Sn nanoparticles. The four peaks at 398.2, 399.9, 401.2, and 402.1 eV in the N 1s spectrum are ascribed to pyridine N, pyrrolic N, graphite N and pyridine N-oxide in the composite, respectively, indicating that the graphene nanosheets are successfully doped by N element (Fig. S2c, ESI†). N-doping could improve the electronic conductivity of graphene nanosheets and lead to the formation of interfacial Sn-N bonds, which are probably indispensable for the high and stable electrochemical performance of the composite.[1a,9] The XPS analysis suggests that about 4.2 at% nitrogen exist in the composite (Fig. 2c). The Raman spectrum (Fig. 2d) of the composite exhibits a D band located around 1346 cm^{-1} and a G band around 1590 cm^{-1}, corresponding to the sp^3 defect sites and sp^2-bonded pairs, respectively.[10] The high intensity ratio of D to G which is about 1.05 and the absence of 2D-band peak suggest that plenty of defects are present in NGNSs derived from the N-doping. Additionally, two small peaks are observed at 211 and 110 cm^{-1}, corresponding to the A_{1g} and B_{1g} vibrational modes of the tetragonal SnO structure, consistent with the result reported in the literature.[11]

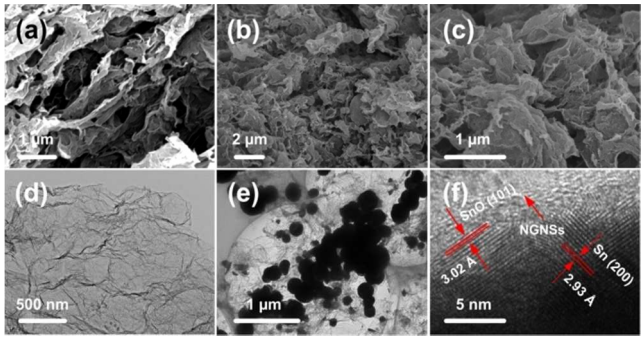

Fig. 3 SEM images of (a) NGNSs and (b, c) Sn/SnO/NGNSs composite. TEM images of (d) NGNSs and (e) Sn/SnO/NGNSs composite. (f) HRTEM image of Sn/SnO/NGNSs composite.

The morphology and structure of the samples were revealed by scanning electron microscopy (SEM) and transmission electron microscopy (TEM). The SEM image shows that the NGNSs have a distinct crumpled structure, thereby forming many voids (Fig. 3a). The crumpled structure can also be observed in the TEM image (Fig. 3d). Sn nanoparticles are clearly observed in the SEM image of the mechanical mixture of Sn nanoparticles and NGNSs (Fig. S4, ESI†). Upon thermal treatment at 250 ºC, these Sn nanoparticles will become molten and penetrate into the crumpled NGNSs, leaving only a few nanoparticles on the surface of the composite (Fig. 3b and c). The TEM image demonstrates that the Sn/SnO nanoparticles are wrapped by a thin layer of NGNSs (Fig. 3e). The poor distribution of nanoparticles might be due to the high surface tension of molten Sn in crumpled NGNSs. In the high-resolution TEM (HRTEM) image of the composite (Fig. 3f), distinct crystal lattices with interplanar distances of 3.02 and 2.93 Å are observed, corresponding well to the (101) plane of SnO and the (110) plane of Sn, respectively. HRTEM image also reveals that SnO is generated on the surface of the Sn nanoparticles, forming a Sn/SnO heterostructure covered by few-layered NGNSs.

Typical cyclic voltammetry (CV) curves of the Sn/SnO/NGNSs composite at a scanning rate of 0.1 mV s^{-1} are shown in Fig. 4a. An irreversible reduction peak at ~0.9 V is observed in the first cathodic scan, attributable to the reduction of SnO into Sn and the formation of solid electrolyte interface (SEI) layer. The cathodic curves below 0.7 V can be ascribed to alloying processes of Sn with lithium. The oxidation peaks at 0.4-0.8 V during the anodic scans can be assigned to the de-alloying reaction of Li_xSn, consistent with Sn-based anodes reported previously.[3,12] Fig. 4b shows the discharge-charge profiles of the composite cycled at a current density of 1.0 A g^{-1} between the potential range of 0.01-3.0 V (*vs.* Li^+/Li). The profiles are typical for Sn-based anodes. The initial discharge and charge capacities are 1081 and 487 mAh g^{-1} (Based on the total mass of composite), respectively, corresponding to a Coulombic efficiency (CE) of 45.0%. The initial irreversible capacity of the

composite might be attributed to the formation of SEI and the utilization of NGNSs, whose first discharge capacity and CE are approximately 905

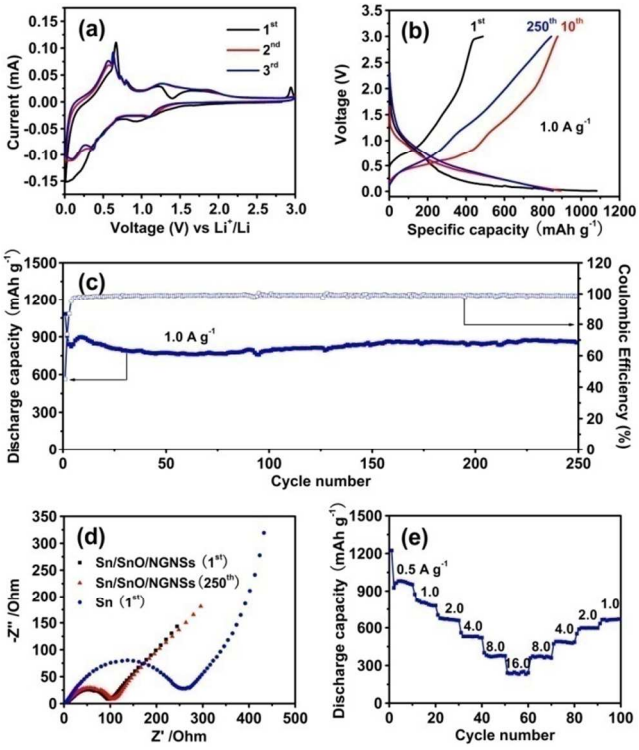

Fig. 4 (a) CV curves, (b) galvanostatic charge-discharge profiles, and (c) cycling performance of the Sn/SnO/NGNSs composite. (d) Nyquist plots of the Sn/SnO/NGNSs and pure Sn electrodes after cycling tests (current density: 1.0 A g^{-1}). (e) Rate capability of the Sn/SnO/NGNSs composite.

mAh g^{-1} and 20.8%, respectively (Fig. S5a, ESI†). The SEM observation of the Sn/SnO/NGNSs electrode after 250 cycles shows that a film covers the surface of the electrode, confirming the generation of SEI (Fig. S5b, ESI†).

The cycling stability of the Sn/SnO/NGNSs composite is evaluated at a current density of 1.0 A g^{-1} (Fig. 4c). After 250 cycles, a high discharge capacity of 853 mAh g^{-1} is obtained, approximately 79.0% of that of the first cycle, demonstrating the excellent cycling stability of the composite. The slightly increase in the capacity in the initial 10 cycles might be associated with the gradual activation of some large Sn/SnO nanoparticles in the composite. Moreover, CE of over 98% is well maintained after the 5th cycle. For comparison, the cycling stability of the mechanical mixture of Sn and NGNSs (Sn/NGNSs-M) and commercial Sn nanoparticles is also evaluated under the same condition (Fig. S6, ESI†). Dramatic capacity decay for the Sn/NGNSs-M is observed upon cycling, particularly for the first 20 cycles. After 50 cycles, a discharge capacity of 443 mAh g^{-1}, approximately 43% of the initial capacity is maintained. For the commercial Sn nanoparticles, only 19% of its initial capacity is retained after 50 cycles. Fig. 4d displays the impendence spectra of the Sn/SnO/NGNSs composite and Sn nanoparticles. The resistance of the composite electrode is much lower than that of pure Sn electrode after the first cycle, indicating that the introduction of NGNSs can significantly enhance the conductivity of the electrode. Furthermore, no obvious increase in the resistance of the composite is observed after discharged/charged for 250 cycles, indicating the excellent structural stability of the composite upon cycling. The rate capability of the Sn/SnO/NGNSs composite at different current densities is shown in Fig. 4e. The corresponding charge-discharge profiles are given in Fig. S7 (ESI†). The discharge capacities of the composite are 1224, 874, 701, 561, 401 and 241 mAh g^{-1} at current densities of 0.5, 1.0, 2.0, 4.0, 8.0 and 16.0 A g^{-1}, respectively. After the high-rate discharge-charge cycling, a discharge capacity as high as 634 mAh g^{-1} is recovered when the current density is decreased stepwise to 1.0 A g^{-1}. The large specific capacity, excellent cycling stability, and high rate capability are attributed to the unique structural features of the composite. First, the remaining empty space among the crumpled NGNSs cannot only facilitate the diffusion of electrolyte and Li^+ into the electrode, but also accommodate the huge volume change of Sn during lithiation/delithiation processes. Second, the introduction of NGNSs can obviously enhance the electronic conductivity of electrode and buffer the large volume change of Sn during cycling. Third, the generation of SnO can ensure good contact between the Sn-based nanoparticles and NGNSs, avoiding the aggregation of the nanoparticles and keeping the structural stability of the composite during cycling.

In summary, a simple melting diffusion method has been developed for the preparation of Sn/SnO/NGNSs composite by the penetration of molten Sn into the void space among the crumpled NGNSs at a temperature of 250 ºC. The as-obtained composite exhibits excellent electrochemical performance for LIBs, ascribed to the synergistic effects combining the introduction of NGNSs, the formation of Sn/SnO heterostructure, and the remaining void space among the crumpled NGNSs. Moreover, the simple melting diffusion method can be extended to the preparation of other electrode materials through rational selection of the appropriate host and guest species, generating functional composite materials with designed structures and morphologies.

This work was financially supported by the National Basic Research Program of China (2013CB934102 and 2014CB932102) and the National Natural Science Foundation of China.

Notes and references

School of Chemistry and Chemical Engineering, Shanghai Jiao Tong University, Shanghai 20040, P. R. China. E-mail: k.wang@sjtu.edu.cn (KXW), weixiao@sjtu.edu.cn (WX)

† Electronic Supplementary Information (ESI) available. See DOI: 10.1039/b000000x/

1 (a) X. Zhou, L. J. Wan and Y. G. Guo, *Adv. Mater.*, 2013, **25**, 2152; (b) M. J. Armstrong, C. O'Dwyer, W. J. Macklin and J. D. Holmes, *Nano Res.*, 2014, **7**, 1.

2 (a) J. Hwang, S. H. Woo, J. Shim, C. Jo, K. T. Lee and J. Lee, *ACS Nano*, 2013, **7**, 1036; (b) B. Luo, B. Wang, M. Liang, J. Ning, X. Li and L. Zhi, *Adv. Mater.*, 2012, **24**, 1405; (c) J. Chen, L. Yang, Z. Zhang, S. Fang and S. Hirano, *Chem. Commun.*, 2013, **49**, 2792.

3 Z. Zhu, S. Wang, J. Du, Q. Jin, T. Zhang, F. Cheng and J. Chen, *Nano Lett.*, 2014, **14**, 153.

4 (a) Y. Yu, L. Gu, C. Wang, A. Dhanabalan, P. A. van Aken and J. Maier, *Angew. Chem., Int. Ed.*, 2009, **48**, 6485; (b) W. M. Zhang, J. S. Hu, Y. G. Guo, S. F. Zheng, L. S. Zhong, W. G. Song and L. J. Wan, *Adv. Mater.*, 2008, **20**, 1160; (c) Y. Qiu, K. Yan and S. Yang, *Chem. Commun.*, 2010, **46**, 8359; (d) K. T. Lee, Y. S. Jung and S. M. Oh, *J. Am. Chem. Soc.*, 2003, **125**, 5652; (e) X. W. Lou, C. M. Li and

L. A. Archer, *Adv. Mater.*, 2009, **21**, 2536; (f) W. Fu, F. H. Du, K. X. Wang, T. N. Ye, X. Wei and J. S. Chen, *J. Mater. Chem. A*, 2014, **2**, 6960.

5 P. Wu, N. Du, J. Liu, H. Zhang, J. Yu and D. Yang, *Mater, Res. Bull.*, 2011, **46**, 2278.

6 X. Ji, K. T. Lee and L. F. Nazar, *Nat. Mater.*, 2009, **8**, 500.

7 (a) X. F. Zhang, K. X. Wang, X. Wei and J. S. Chen, *Chem. Mater.*, 2011, **23**. 5290; (b) H. J. Zhang, K. W. Wang, X. Y. Wu, Y. M. Jiang, Y. B. Zhai, C. Wang, X. Wei and J. S. Chen, *Adv. Funct. Mater.*, 2014, **24**, 3399.

8 Z. Wen, X. Wang, S. Mao, Z. Bo, H. Kim, S. Cui, G. Lu, X. Feng and J. Chen, *Adv. Mater.*, 2012, **24**, 5610.

9 X. Zhou, J. Bao, Z. Dai and Y. G. Guo, *J. Phys. Chem. C* 2013, **117**, 25367.

10 Z. L. Wang, D. Xu, Y. Huang, Z. Wu, L. M. Wang and X. B. Zhang, *Chem. Commun.*, 2012, **48**, 976.

11 M. Z. Iqbal, F. Wang, H. Zhao, M. Y. Rafique, J. Wang and Q. Li, *Scr. Mater.*, 2012, **67**, 665.

12 Y. Xu, J. Guo and C. Wang, *J. Mater. Chem.*, 2012, **22**, 9562.